

Controlling the interfacial dipole via functionalization of quinoxaline-based small molecules for electron transport layer in organic light emitting diodes

Seok Woo Lee, Xiangyang Fan, Dong Ryeol Whang, Ji Won Jang, Hyosung Choi, Dong Wook Chang & Bo Ram Lee

To cite this article: Seok Woo Lee, Xiangyang Fan, Dong Ryeol Whang, Ji Won Jang, Hyosung Choi, Dong Wook Chang & Bo Ram Lee (2023): Controlling the interfacial dipole via functionalization of quinoxaline-based small molecules for electron transport layer in organic light emitting diodes, Journal of Information Display, DOI: [10.1080/15980316.2023.2171145](https://doi.org/10.1080/15980316.2023.2171145)

To link to this article: <https://doi.org/10.1080/15980316.2023.2171145>



© 2023 The Author(s). Published by Informa UK Limited, trading as Taylor & Francis Group on behalf of the Korean Information Display Society



Published online: 02 Feb 2023.



Submit your article to this journal [↗](#)



Article views: 235



View related articles [↗](#)



View Crossmark data [↗](#)

Controlling the interfacial dipole via functionalization of quinoxaline-based small molecules for electron transport layer in organic light emitting diodes

Seok Woo Lee^{a,e,*}, Xiangyang Fan^{b,e,*}, Dong Ryeol Whang^c, Ji Won Jang^d, Hyosung Choi^d, Dong Wook Chang^{a,e} and Bo Ram Lee^{b,e}

^aDepartment of Industrial Chemistry, Pukyong National University, Busan, Republic of Korea; ^bDepartment of Physics, Pukyong National University, Busan, Republic of Korea; ^cDepartment of Advanced Materials, Hannam University, Daejeon, Republic of Korea; ^dDepartment of Chemistry, Research Institute for Convergence of Basic Science, and Research Institute for Natural Sciences, Hanyang University, Seoul, Republic of Korea; ^eCECS Research Institute, Core Research Institute, Busan, Korea

ABSTRACT

Optoelectronic devices with organic semiconductors, such as organic light-emitting diodes (OLEDs), have received much attention because they offer ease of processing and device flexibility. However, practical application of these devices is still hindered by relatively poor device performance and lack of cost-effective fabrication process, which represent properties largely determined by the molecular dipole moments of the organic molecules. In this study, we designed and prepared novel quinoxaline-phosphine oxide small molecules (QPSMs) as the electron transport layer (ETL) for the solution-processable OLEDs by tuning the end functional group of the aromatic QPSMs. A key design criterion was controlling the dipole moments of QPSMs, which confers (1) convenient deposition on the emission layer without further annealing through solubility in isopropanol and (2) improved electron injection/transport behavior through effective band level matching of the devices. In particular, the optimized OLEDs with (4-(2,3-bis(4-methoxyphenyl)quinoxalin-5-yl)phenyl)diphenylphosphine oxide (MQxTPPO1) exhibit external quantum efficiency (EQE) of 6.12%. Our results demonstrate the potential application of QPSMs as next-generation ETLs in organic semiconductors.

ARTICLE HISTORY

Received 14 November 2022
Accepted 10 January 2023

KEYWORDS


Small molecule; solution process; organic optoelectronic device

1. Introduction

Over the past decades, organic light-emitting diodes (OLEDs) have attracted enormous attention owing to their cost-effectiveness, good mechanical flexibility, and promising potential for scalable roll-to-roll technology [1–6]. The development of a low temperature, inexpensive, and scalable solution-based fabrication process is of utmost importance in the commercial applications OLEDs [7–9]. However, traditional electron transport layers (ETLs) such as barium (Ba) [10] and calcium (Ca) [11] as well as electron injection layers (EILs) including lithium fluoride (LiF) [12] and cesium carbonate (Cs₂CO₃) [13,14], which usually consist of metal-based low-work-function (LWF) materials in OLEDs and significant barrier toward commercialization [15]. These materials require not only laborious high temperature vacuum deposition but also supplementary

encapsulating layers for minimizing device corruption induced by undesirable contact with oxygen and moisture [16,17].

To mitigate this issue, solution-processable inorganic *n*-type metal oxides, such as titanium oxide (TiO_x) [18], zinc oxide (ZnO) [19], and zirconium dioxide (ZrO₂) [20], have been considered as possible alternatives to LWF ETLs. While these oxides demonstrate high electron mobilities, exceptional chemical stability, and good electrical and mechanical robustness, there are large injection barriers between these *n*-type metal oxides and the active layer. Consequently, additional surface modification or interface engineering using functional molecules such as conjugate polymer electrolytes and ionic liquids are usually applied to modulate the energy level of the corresponding devices [21–24]. Furthermore, the solution processing of *n*-type metal oxides with high crystallinity

CONTACT Dong Wook Chang  dwchang@pknu.ac.kr  Department of Industrial Chemistry, Pukyong National University, Busan 48547, Republic of Korea CECS Research Institute, Core Research Institute, Busan, Korea; Bo Ram Lee  brlee@pknu.ac.kr Department of Physics, Pukyong National University, Busan 48547, Republic of Korea CECS Research Institute, Core Research Institute, Busan, Korea

* These authors contributed equally to this work.

ISSN (print): 1598-0316; ISSN (online): 2158-1606

© 2023 The Author(s). Published by Informa UK Limited, trading as Taylor & Francis Group on behalf of the Korean Information Display Society
This is an Open Access article distributed under the terms of the Creative Commons Attribution-NonCommercial License (<http://creativecommons.org/licenses/by-nc/4.0/>), which permits unrestricted non-commercial use, distribution, and reproduction in any medium, provided the original work is properly cited.

must rely on high temperature annealing above 400°C, which typically degrades (polymer-based) flexible substrates.

To solve these problems issued from LWF materials and inorganic metal oxides, considerable efforts have been paid to the development of alternative ETLs based on organic compounds, which in principle solves many of the problems faced by metal oxide ETLs [25,26]. Normally, *n*-type organic ETLs are composed of electron-deficient nitrogen-containing heteroaromatics and/or phosphine oxide moieties with a larger bandgap of over 3.0 eV [27,28]. In addition, the lower values of both lowest unoccupied molecular orbital (LUMO) and highest occupied molecular orbital (HOMO) energy levels are preferred to enhance electron injecting and hole blocking capabilities of organic ETLs, respectively. Unfortunately, most common organic ETLs such as (4-Biphenyl)-5-(4-tert-butylphenyl)-1,3,4-oxadiazole (PBD) [29], 3-(Biphenyl-4-yl)-5-(4-tert butylphenyl)-4-phenyl-4H-1,2,4-triazole (TAZ) [30], 2,2',2''-(benzene-1,3,5-triyl)-tris(1-phenyl-1H-benzimidazole) (TPBi) [31–33], and 2,9-dimethyl-4,7-diphenyl-1,10-phenanthroline (BCP) [34,35] still mainly rely on the complicated thermal evaporation process under high vacuum condition. The development of solution-processable organic ETLs with good electron mobility, enhanced stability, and facile solution processability at low temperature is still in its infancy [36].

The problem of solution-processable organic ETLs arises from the dipole moment of the molecular species. While the solubilities of organic ETLs in organic solvents predominantly rely on the dipolar moment, these same dipole moments of organic ETLs also play important roles in enhancing device performances, because the work function (WF) of the adjacent cathode can be favorably tuned by the generation of large interfacial dipoles between ETL and cathode [37–42]. In this condition, the energy barrier at the interface between the active layer and cathode can be efficiently reduced by the insertion of organic ETLs, leading to better electron injection from the cathode to the active layer.

Recently, our group reported the quinoxaline-phosphine oxide-based small molecules (QPSMs) named as QxTPPO1 and QxTPPO2 to be used for the solution processable ETLs in optoelectronic devices [43]. Owing to the careful design of the molecular dipole moment with the triphenyl phosphine oxide group as a prominent functional group, these QPSMs can not only exhibit good solubility in alcoholic solvents but also efficiently modulate the WF of cathodes [44,45]. Hence, the application of QxTPPO1 and QxTPPO2 as ETLs can improve the device performances of polymer solar cells and OLEDs by promoting the electron injection/transport processes.

However, more delicate controls on the properties of QPSM-based molecular structures such as energy level, solubility, and dipole moment are still required to achieve even higher performance organic ETLs.

In this study, two novel QPSMs were developed and tested as solution-processable ETLs in OLEDs by adopting the structure of QxTPPO1 as a reference building block. With an aim to design and tune the dipole moment and its related properties of QxTPPO1, the type of substituents at the *para*-positions of phenyl ring on the 2,3-positions of quinoxaline unit were systematically varied. The resulting QPSM molecules show better solubility in alcoholic solvents, in addition to enhanced energy level matching with the organic polymer active layer.

2. Results and discussion

To demonstrate the extremities of functional group modulation, we have selected an electron-donating methoxy (OCH₃) unit and an electron-withdrawing fluorine (F) atom to substitute for the hydrogen atoms as described above. This affords two QPSMs denoted as (4-(2,3-bis(4-methoxyphenyl)quinoxalin-5-yl)phenyl)diphenylphosphine oxide (MQxTPPO1) and (4-(2,3-bis(4-fluorophenyl)quinoxalin-5-yl)phenyl)diphenylphosphine oxide (FQxTPPO1), respectively. The chemical structures of QxTPPO1, MQxTPPO1, and FQxTPPO1 are shown in Figure 1a. Interestingly, despite their similar parental backbone, MQxTPPO1 and FQxTPPO1 exhibited quite different optical, electrochemical, and crystallinities, which mainly stem from the opposite electronic effects of two substituents (electron-withdrawing –F and electron-donating –OCH₃). In particular, the dipole moments of the two QPSMs also varied significantly with respect to the substituent group (7.46 D to 2.83 D, see below).

Similar to the QxTPPO1 reference, MQxTPPO1 and FQxTPPO1 are soluble in alcohol solvents, so they can be easily casted as ETLs in optoelectronic devices via a simple solution-based spin-coating process. The performance of MQxTPPO1 and FQxTPPO1 as a function of ETL was analyzed by fabricating the OLED device with a structure of indium tin oxide (ITO)/poly(3,4-ethylenedioxythiophene):poly(styrenesulfonate) (PEDOT:PSS)/Super Yellow (SY)/QPSMs/ Al (Figure 1b). The chemical structure of SY as an emissive layer was shown in Figure 1c [46,47]. Notably, the device based on MQxTPPO1 exhibited the highest external quantum efficiency (EQE) of 6.12%, compared to those of the devices based on QxTPPO1 reference (5.65%) and FQxTPPO1 (2.94%). The best EQE of the device based on MQxTPPO1 was attributed to an increase in the electron injection/transporting process derived from its crystalline structure and largest dipole moment. Therefore,

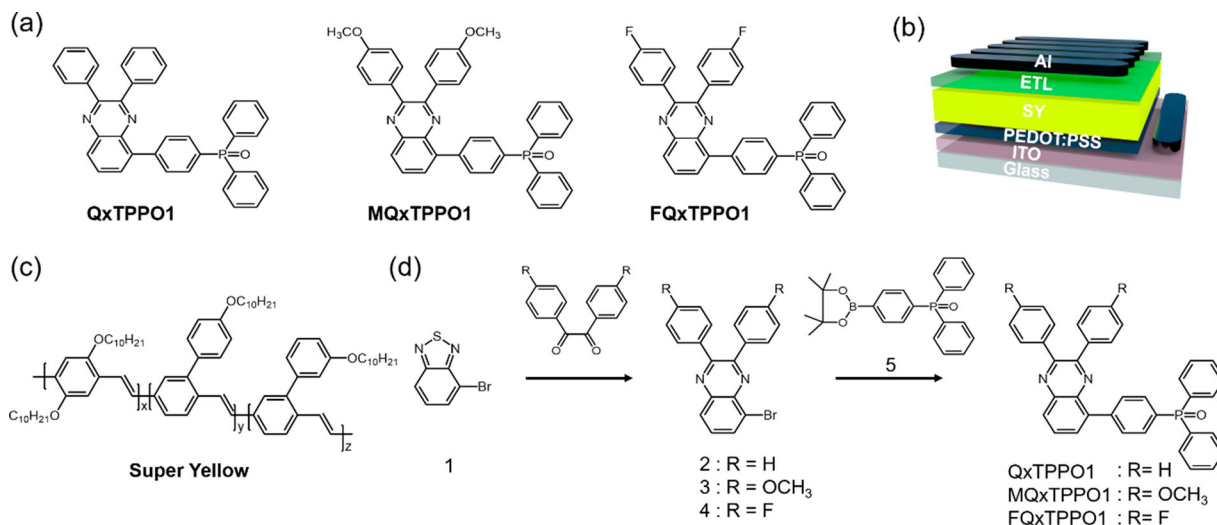


Figure 1. (a) Chemical structures of QPSMs, (b) device configuration, (c) chemical structures of SY, and (d) synthesis schemes for the QPSMs.

these results can provide useful insights into the substitution effects of the electron-donating and electron-withdrawing moieties in *n*-type QPSMs as an interlayer of OLEDs.

The synthetic procedures for MQxTPPO1 and FQxTPPO1 are shown in Figure 1d, while the detailed synthetic procedure, ¹H-NMR, ¹³C-NMR, and mass spectrometric data are described in the Electronic Supplementary Information (ESI). Firstly, QxTPPO1 reference, 4-bromobenzo[*c*][1,2,5]thiadiazole (1) and diphenyl(4-(4,4,5,5-tetramethyl-1,3,2-dioxaborolan-2-yl)phenyl) phosphine oxide (5) were prepared according to the previous report [43]. Secondly, the sequential reactions of reduction by zinc and condensation with α -diketone afforded the mono-brominated quinoxaline intermediates (3 and 4). Particularly, the use of *p*-anisil and 4,4'-difluorobenzil as α -diketones can simply introduce the electron-donating OCH₃ and electron-withdrawing F substituents at the *para*-position of phenyl rings on the 2,3-positions of quinoxaline unit. Finally, the Suzuki coupling reaction of 3 and 4 with 5 can produce the target QPSMs of MQxTPPO1 and FQxTPPO1, respectively. The thermal characteristics of QPSMs were analyzed using thermogravimetric analysis (TGA) and differential scanning calorimetry (DSC) measurements. As shown in Figure 2a, TGA thermograms exhibited thermal stability of QPSMs up to 300°C, with the onset decomposition temperatures at 5 wt% weigh loss ($T_{d5\%}$) for QxTPPO1, MQxTPPO1, and FQxTPPO1 to be 333, 356, and 332°C, respectively. In addition, the melting points (T_m) of 219 and 165°C were monitored from the DSC thermograms of QxTPPO1 and MQxTPPO1, respectively (Figure 2b). The presence of bulky OCH₃ substituents can hinder intermolecular interactions, which significantly reduce

T_m of MQxTPPO1 compared to that of QxTPPO1 reference. On the contrary, no clear T_m was observed from the DSC thermogram of FQxTPPO1, suggesting its amorphous nature. The obvious differences between the crystalline structures of QPSMs were also confirmed by X-ray diffraction (XRD) analysis. As shown in Figure 2c, the powders of QxTPPO1 and MQxTPPO1 exhibited the typical XRD patterns of polycrystalline samples, while that of FQxTPPO1 only displayed featureless broad peak [48,49]. The different crystallinities of these two molecular solids may originate from their dipolar moments, which depend on the substituents at the *para*-position of phenyl rings on the 2,3-positions of quinoxaline unit: less polar FQxTPPO1 may be more prone to random packing, unlike strongly polar MQxTPPO1 where the molecules are more likely to 'line up' according to their dipoles [50].

The ultraviolet-visible (UV-Vis) absorption rates of QxTPPO1, MQxTPPO1, and FQxTPPO1 in solution state are shown in Figure 2d. All compounds displayed similar absorption peaks in the range between 310–400 nm, which can be assigned to the π - π transition of the conjugated backbone. The absorption peak of MQxTPPO1 was slightly red-shifted around 10 nm compared to those of QxTPPO1 and FQxTPPO1, due to the reduced bandgap. Moreover, Tauc plots in film state were plotted to determine the optical bandgap, and the values for QxTPPO1, MQxTPPO1, and FQxTPPO1 were calculated to be 3.18, 2.98, and 3.15 eV, respectively (Figure S1 in ESI). The highest occupied molecular orbital (HOMO) and lowest unoccupied molecular orbital (LUMO) energy levels of QPSMs were investigated using cyclovoltammetry (CV) measurement in the presence of a ferrocene standard (Figure 2e). The calculated HOMO/LUMO energy

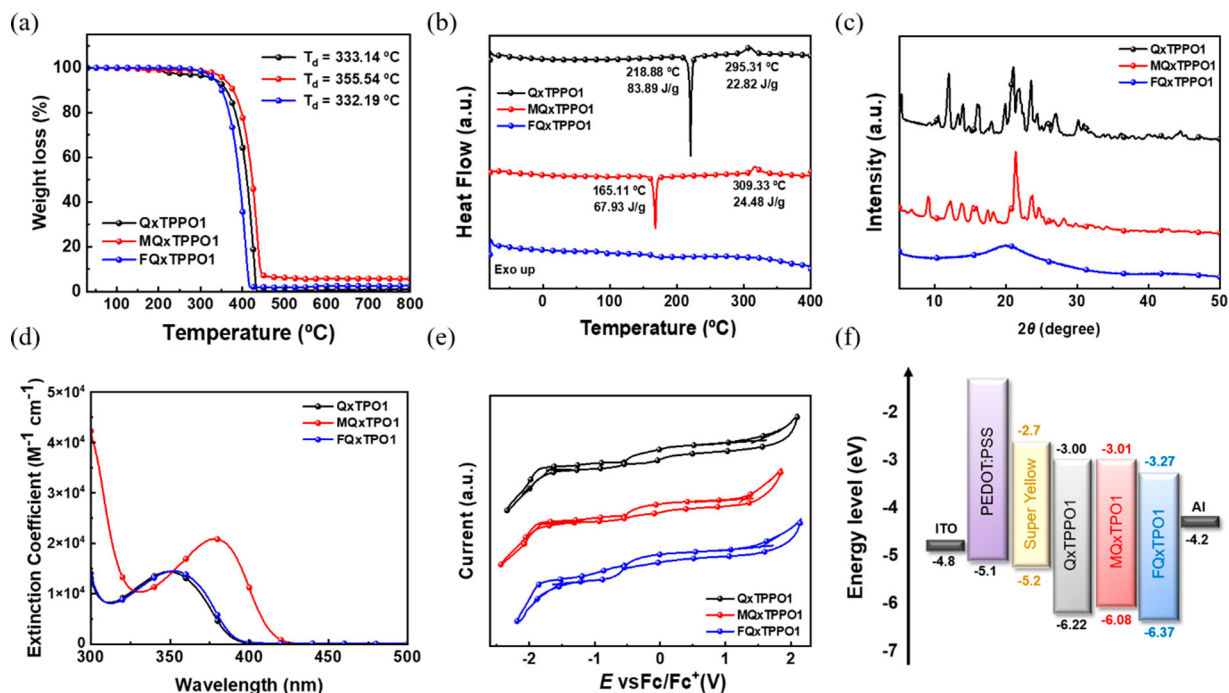


Figure 2. (a) TGA thermograms, (b) DSC thermograms, and (c) XRD data of QxTPPO1, MQxTPPO1, and FQxTPPO1, (d) UV-vis spectra in the chloroform solution, (e) CV curves of QxTPPO1, MQxTPPO1, and FQxTPPO1, and (f) Energy diagrams of all materials in the OLEDs.

Table 1. Optical and electrochemical properties of QPSMs.

Polymer	λ_{max}^{abs} (nm) ^a	E_{gap}^{opt} (eV) ^b	HOMO (eV) ^c	LUMO (eV) ^d	E_{gap}^{elec} (eV) ^e
QxTPPO1	349	3.18	-6.22	-3.00	3.22
MQxTPPO1	379	2.98	-6.08	-3.01	3.07
FQxTPPO1	352	3.15	-6.37	-3.27	3.10

Note: ^aMaximum absorption peak in the chloroform solution; ^bEstimated from Tauc plot in thin film state; ^cEstimated by the oxidation onset potential; ^dEstimated by the reduction onset potential; ^eCalculated by the oxidation and reduction onset potentials in the CV curves.

levels for QxTPPO1, MQxTPPO1, and FQxTPPO1 were -6.22/-3.00, -6.08/-3.01, and -6.37/-3.27 eV, respectively. Notably, the incorporation of electron-donating OCH₃ unit significantly increased the HOMO energy levels of MQxTPPO1, whereas the loading of electron-withdrawing F atom diminished the HOMO energy levels of FQxTPPO1 with respect to that of QxTPPO1 reference [51]. The electrochemical bandgaps of QxTPPO1, MQxTPPO1, and FQxTPPO1 from CV measurement were calculated at 3.22, 3.07, and 3.10 eV, respectively. The trend in electrochemical bandgaps of QPSMs agrees well with that in the optical bandgaps, and all the optical and electrochemical properties of QPSMs are presented in Table 1. Based on these results, the favorable charge transfer in the fabricated OLEDs was supported by the energy diagrams of all device components (Figure 2f).

Density functional theory (DFT) calculations were performed using the Gaussian 16 program at the B3LYP/6-31G** level to predict the frontier molecular

orbitals, optimized geometries, and molecular dipole moments of the QPSMs [52]. Firstly, all QPSMs showed quite distinct electron density distributions to each other in both LUMO and HOMO energy levels, representing the significant contributions of the electron-donating and electron-withdrawing substituents on the electronic structures of QPSMs (Figure S2 in ESI). In addition, FQxTPPO1 exhibited the deepest LUMO and HOMO energy levels, while MQxTPPO1 showed the shallowest LUMO and HOMO energy levels. These results coincide with those obtained from the electrochemical analysis. Secondly, molecular dipole moments of the QPSMs at their optimized geometries were determined, and the results are shown in Figure 3a. The direction and magnitude of each molecular dipole moment is highly susceptible to the molecular structures, with the calculated values for QxTPPO1, MQxTPPO1, and FQxTPPO1 at 4.78, 7.46, and 2.83 Debye (D), respectively. MQxTPPO1 showed the largest dipole moment, due to the strengthened push-pull interactions caused by the presence of the electron-donating -OCH₃ unit at the *para*-position of phenyl ring. On the contrary, the introduction of the electron-withdrawing F atoms at the same position seriously deteriorates the push-pull interactions, consequently reducing the net dipole moment of FQxTPPO1.

It has been reported that the generation of interfacial dipoles by fabricating the electron-transporting materials with high dipole moment can efficiently tune the work function (WF) of the electrode (Figure 3b) [38]. In this

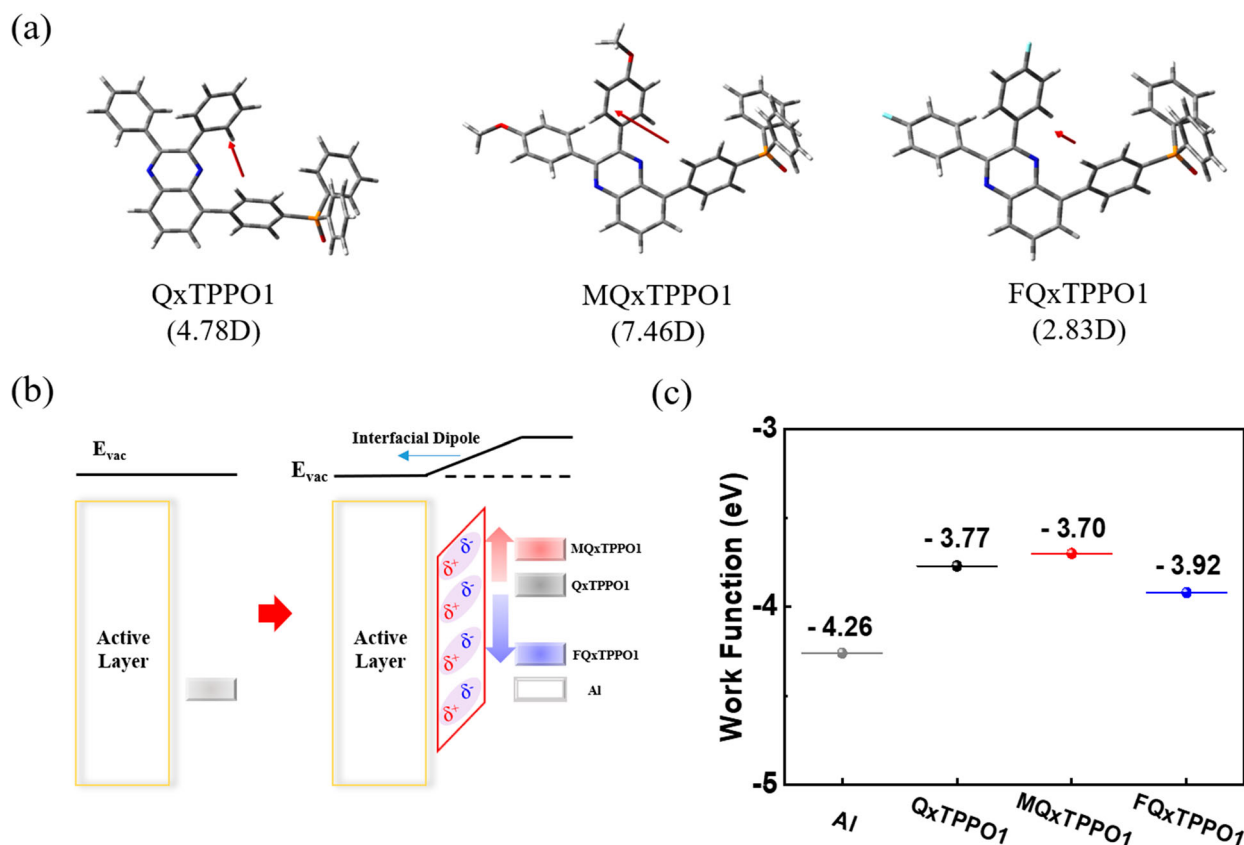


Figure 3. (a) Optimized geometry with the value of dipole moment of QxTPPO1, MQxTPPO1, and FQxTPPO1, (b) Schematic images of interfacial dipole moment and (c) Cathode work functions with and without ETL (scanning Kelvin probe measurement).

regard, the WF of Al electrode with different QPSMs-based ETLs were measured using a Kelvin probe, which is used widely in estimating the WF of semiconductors. As depicted in Figure 3c, the unmodified Al electrode displayed the typical WF of -4.26 eV, whereas the modified Al electrodes with QxTPPO1, MQxTPPO1, and FQxTPPO1 exhibited the WF values of -3.77 , -3.70 , and -3.92 eV, respectively. Although all QPSMs can readily shift the WF of the electrode, the deviation from pristine Al electrode is strongly proportional to the strength of their molecular dipole moments. The smaller energy barrier between the active layer and electrode is usually preferred in OLEDs, because the electron injection from electrode to active luminescent material can be facilitated in this condition. Therefore, the best performance can be anticipated from the device with MQxTPPO1 through the enhanced charge injection and charge transporting process.

To observe the effect of electron transport according to the changed work function after coating QPSMs, the electron-only devices similar to OLEDs were fabricated, as shown in Figure S3 [53]. The device configuration of the electron-only device is ITO/ZnO/PEI/SY/QPSMs/Al used ZnO and PEI instead of PEDOT:PSS. In the

electron-only devices, it is seen that the current density of MQxTPPO1 is higher than that of QxTPPO1, while the current density of FQxTPPO1 used electron-withdrawing group is lower than that of QxTPPO1. This result indicates that electron injection and transport are significantly increased when MQxTPPO1 is used as the ETL, which results from the reduced energy barrier between the emissive layer and ETL. The behavior of electron injection/transport is in good agreement with the change in work function obtained from the Kelvin Probe and with the predicted DFT results above. The device performances of OLEDs with three QPSMs are shown in Figure 4a–d. In Figure 4a, the current density of OLEDs without QPSMs is lower than other devices with QPSMs, which is attributed to poor electron injection and transport due to the existing large energy barrier between SY and Al.

The improved electron injection/transport in OLEDs with QPSMs leads to a dramatic enhancement of OLED device performance compared to the device without QPSMs. The optimized OLEDs using QxTPPO1 without additional substituents showed luminescence values of 6211 cd/m^2 , luminous efficiency (LE) of 16.69 cd/A , and EQE of 5.65% . In particular, the best OLEDs

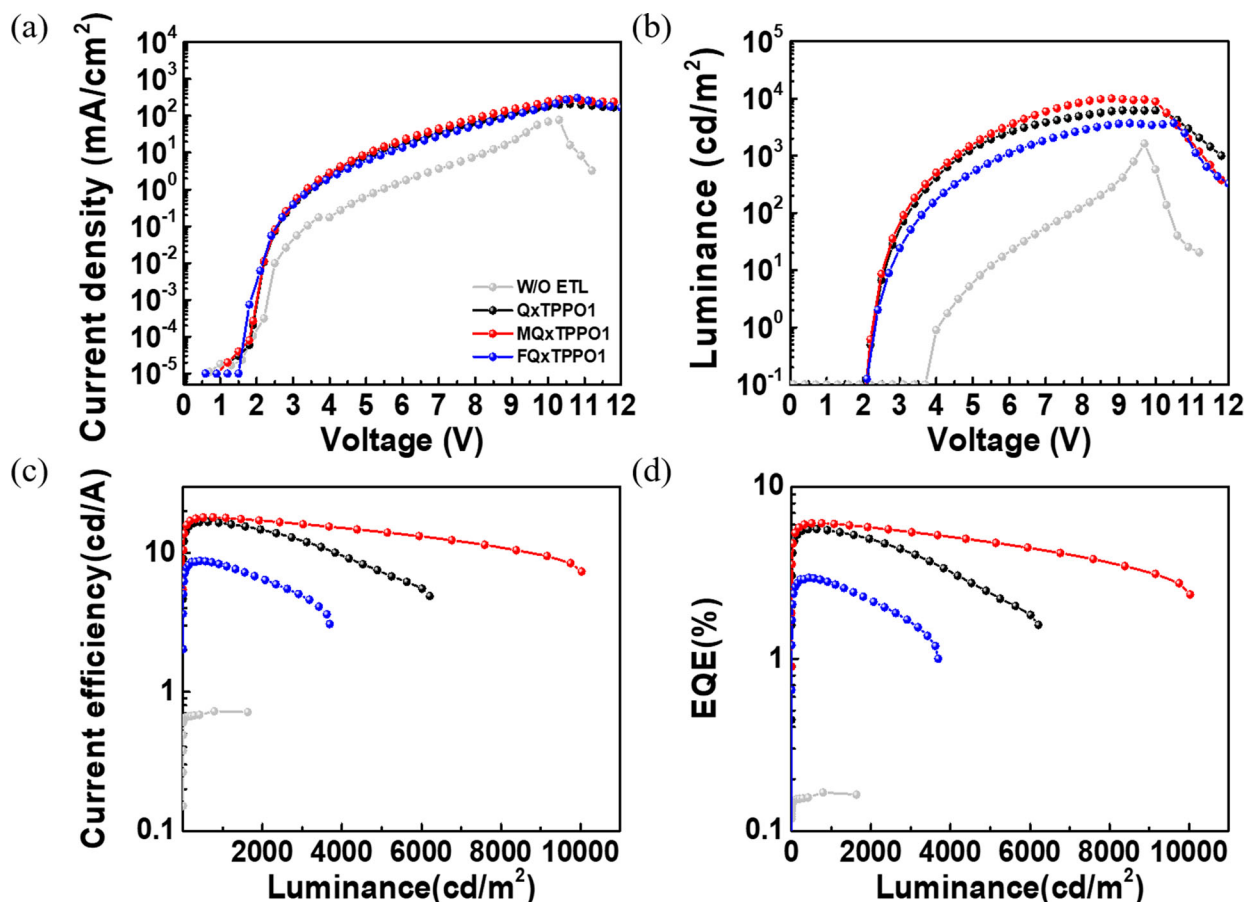


Figure 4. Device performance of OLEDs with QPSMs; (a) J-V curves, (b) L-V curves, (c) LE-L curves, and (d) EQE-L.

Table 2. Summarized device performance for OLEDs.

Device configuration(OLEDs)	L_{\max} [cd/m ²] @ bias	LE_{\max} [cd/A] @ bias	EQE_{\max} [%] @ bias	Turn-on Voltage [V] @ 1cd/m ²
ITO / PEDOT:PSS / SY / Al	1633@9.7	0.72@9.4	0.16@9.4	4.0
ITO / PEDOT:PSS / SY / QxTPPO1 / Al	6211@9.1	16.69@4.3	5.65@4.3	2.5
ITO / PEDOT:PSS / SY / MQxTPPO1 / Al	10030@8.8	17.98@4.3	6.12@4.3	2.5
ITO / PEDOT:PSS / SY / FQxTPPO1 / Al	3723@10.5	8.76@4.8	2.94@4.8	2.5

using MQxTPPO1 show improved luminescence of 10,030 cd/m², LE of 17.98 cd/A, and EQE of 6.12% owing to the minimized energy barrier between SY and Al. On the other hand, OLEDs using FQxTPPO1 substituted with fluorine groups show reduced luminance of 3723 cd/m², LE of 8.76 cd/A and EQE of 2.94%, and these are attributed to the small changes in the energy barrier between SY and Al for the devices with QxTPPO1, MQxTPPO1, FQxTPPO1 and without ETL, respectively. Corresponding efficiency roll-off is 4.07, 0.98, 8.50 and 3.00, respectively, indicating that the efficiency roll-off of MQxTPPO1 has been obviously suppressed. Thus, the device performance of OLEDs is consistent with the electron injection/transport results, which depends on the tendency of the cathode work function to be tuned through induced dipole moments of QPSMs. The details

of the device performance of OLEDs are summarized in Table 2.

To demonstrate the long-term operation stability of OLEDs depending on ETLs, stability measurement was conducted per 50 h under ambient condition without encapsulation, as shown in Figure S4. The operation stabilities determined by the luminance to decay to 50% of its initial value ($L/L_0 = 0.5$) show approximately 70, 320, 500 and 645 h in OLEDs for the control, FQxTPPO1, QxTPPO1, and MQxTPPO1 devices, respectively. The long-term operation stability of OLEDs with MQxTPPO1 is better than that of other OLEDs devices, and is attributed to well-balanced charge transport [54].

Finally, the morphologies of the super yellow (SY) films as active layer with and without QPSMs were

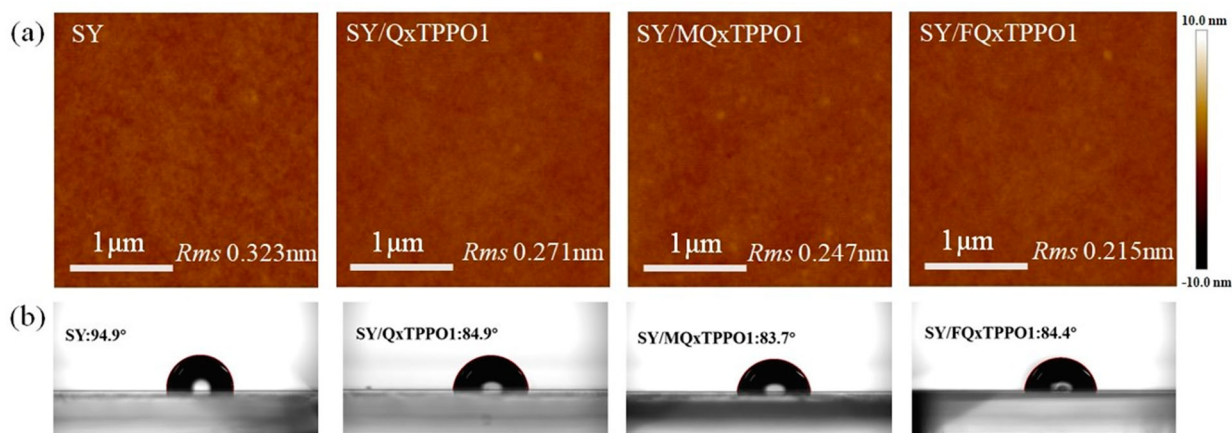


Figure 5. (a) Atomic force microscopy (AFM) images and (b) Contact angles on the SY with and without QSPMs such as QxTPPO1, MQxTPPO1 and FQxTPPO1.

measured by atomic force microscopy to confirm the stability of the active layer. Compared to the roughness of SY without QSPMs, the roughness of QxTPPO1, MQxTPPO1 and FQxTPPO1 are 0.271, 0.247 and 0.215 nm, respectively, manifesting only a negligible change after coating the QSPMs. Overall, smooth and uniformly dispersed surface morphologies are observed, as shown in Figure 5a. We also note that while the contact angles of the SY layer with QSPMs are somewhat different from that without QSPMs (Figure 5b), which are potentially due to the surface morphologies and/or dipole moments, all three samples with QSPMs show similar contact angles.

3. Conclusion

In summary, a series of novel QSPMs containing quinoxaline and their derivatives were newly designed for ETLs, and the WF was controlled by introducing a strong dipole moment via molecular design. The electron injection/transport was also improved in the QSPMs based device due to the well-matched energy levels in the OLEDs. As a result, the MQxTPPO1-based OLEDs yielded external quantum efficiency (EQE) of 6.12%, which delivered greatly enhanced device performance.

4. Experimental

4.1. Materials and instruments

All reagent and solvents were purchased from Sigma Aldrich Chemical Co., Inc. 4-bromobenzo[*c*][1,2,5]thiadiazole (1) and diphenyl(4-(4,4,5,5-tetramethyl-1,3,2-dioxaborolan-2-yl)phenyl)phosphine oxide (5) were produced according to previously reported methods. ^1H and ^{13}C nuclear magnetic resonance (NMR) spectra

were measured using a JEOL JNM ECP-400 spectrometer. UV-visible spectra were recorded on a Lamda 365 spectrophotometer. Gas Chromatography/Mass Spectrometer (GC/MS) was analyzed by using Agilent 7890GC/5975C MSD. Thermogravimetric Analysis (TGA) was measured using Q500 instrument and the work function was measured by Kelvin Probe (equipment number). Differential scanning calorimetry (DSC) was measured Q200 instrument, while x-ray diffractometry (XRD) was carried out using X'Pert3-Powder (PANalytical). Cyclic voltammetry (CV) measurements were carried out by using a Versa STAT3 (AMETEK, Inc.) with tetrabutylammonium hexafluorophosphate (0.1M, Bu_4NPF_6) as the electrolyte in anhydrous acetonitrile. For CV measurements, a glassy carbon electrode coated with the polymer and a platinum wire were used as the working and counter electrode, respectively. A silver wire was used as a pseudo-reference electrode with a ferrocene (Fc)/ferrocenium(Fc^+) external standard.

4.2. Devices fabrication and characterization of OLEDs

ITO-coated glass substrates were cleaned using an ultrasonification process in deionized water, acetone and isopropanol for 10 min. Poly(3,4-ethylenedioxythiophene):poly(styrenesulfonate) (PEDOT:PSS, AI 4083, Clevios) solution (filtered through a 0.45 μm CA filter) was spin-coated at 4000 rpm for 45 s onto the ITO substrate then annealed at 150°C for 10 min. Poly(phenyl vinylene):SY (Merck Co., $M_w = 1,950,000 \text{ g mol}^{-1}$) solution dissolved in chlorobenzene (0.7 wt%) was spin-coated at 2000 rpm for 45 s onto PEDOT:PSS for the emissive layer. The QSPMs solution dissolved in Isopropyl Alcohol (99.9%) was also spin-cast at 2000 rpm for 45 s onto SY, then Al (100 nm) was thermally evaporated for

the cathode under vacuum conditions ($< 10^{-6}$ Torr). The J-V-L characteristics and efficiencies were measured using a Keithley 2450 Source Meter and a Konica Minolta spectroradiometer (CS-2000), respectively.

Disclosure statement

No potential conflict of interest was reported by the author(s).

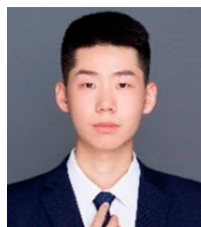
Funding

This work was supported by the National Research Foundation of Korea (NRF - 2022R1A2C4002248, 2021R1A2C1003755, and 2021M3H4A1A02049006). This was also supported by the core research institute (CRI) program, the basic science research program through the National Research Foundation of Korea (NRF) under program number (2022R1A6A1A03051158).

Notes on contributors



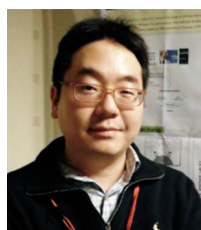
Seok Woo Lee is currently a Research Assistant at CECS Research Institute at the core research institute of Pukyong National University, South Korea. In 2019, he started his research career with Prof. Dong Wook Chang. He intends to pursue a Ph.D. with his research interests involving the synthesis of organic semiconductors for optoelectronic and photovoltaic applications.



Xiangyang Fan is currently a Ph.D. student in the Department of Physics at Pukyong National University, South Korea. In 2020, he started his research career with Prof. Bo Ram Lee. His research interests include organic-inorganic hybrid perovskite light-emitting diodes.



Ji Won Jang is currently a Ph.D. student at the Department of Chemistry at Hanyang University, South Korea. In 2015, she started her research career with Prof. Hyosung Choi. Her research interests include the synthesis of organic-inorganic perovskite materials and device fabrication.



Dong Ryeol Whang has been an associate professor in the Department of Advanced Materials at Hannam University, South Korea, since September 2020. He obtained his Bachelor's, Master's, and Ph.D. degrees from the Department of Material Science & Engineering at Seoul National University in South Korea. Currently, his research interests include the design and synthesis of photosensitizers and catalysts, and methodologies for synthesis, surface modification, and ink formulation of quantum dots for electroluminescent quantum dot light-emitting diodes.



Hyosung Choi has been an associate professor in the Department of Chemistry at Hanyang University, South Korea, since March 2015. He obtained his Bachelor's degree from the Department of Organic Material Science and Engineering at Pusan National University and a Master's degree from the Department of Materials Science and Engineering at Gwangju Institute of Science and Technology (GIST) in South Korea. In 2010, he joined Prof. Jin Young Kim's group and obtained his Ph.D. from the Department of Energy Engineering at the University of Ulsan National Institute of Science and Technology (UNIST), South Korea, in 2013. Currently, his research interests include synthesizing materials and fabricating perovskite and quantum dots solar cells, and device application using hybrid nanomaterials.



Dong Wook Chang has been a professor in the Department of Industrial Chemistry at Pukyong National University, South Korea, since September 2014. He obtained his Bachelor's and Master's degree from the Department of Fiber and Polymer Engineering at Seoul National University in South Korea. In 2003, he joined Prof. Liming Dai's group and obtained his Ph.D. from the Department of Materials Engineering at the University of Dayton, USA, in 2007. Currently, his research interests include the synthesis and functionalization of organic semiconductors and carbon-based nanomaterials for optoelectronic, photovoltaic, energy conversion, and energy storage applications.



Bo Ram Lee has been an associate professor in the Department of Physics at Pukyong National University, Republic of Korea from 2017 to present. He received his Ph.D. degree (2015) from the Department of Materials Science and Engineering of Ulsan National Institute of Science and Technology (UNIST), Republic of Korea. He joined the Optoelectronic Group of the Cavendish Lab, University of Cambridge, as a research associate (2015–2017). His main research fields are organic/polymeric materials and organic – and metal halide perovskite-based optoelectronic devices such as light-emitting diodes and solar cells.

Author contributions

S.W.L., B.R.L. and D.W.C. designed the project and synthesized QPSMs. X.F. conducted device fabrications and general characterizations. D.R.H. contributed to the DFT calculations. J.W.J. and H.C. performed AFM and contact angle analysis. D.W.C. and B.R.L. supervised the project. S.W.L. curated data and wrote the manuscript. D.W.C. and B.R.L. revised and prepared the manuscript.

References

- [1] C. Keum, C. Murawski, E. Archer, S. Kwon, A. Mischok, and M.C. Gather, *Nat. Commun.* **11** (2020).

- [2] M.A. Fusella, R. Saramak, R. Bushati, V.M. Menon, M.S. Weaver, N.J. Thompson, and J.J. Brown, *Nature* **585**, 379–382 (2020).
- [3] M. Singh, H.M. Haverinen, P. Dhagat, and G.E. Jabbour, *Adv. Mater.* **22**, 673–685 (2010).
- [4] R.H. Friend, R.W. Gymer, A.B. Holmes, J.H. Burroughes, R.N. Marks, C. Taliani, D.D.C. Bradley, D.A. dos Santos, J.L. Brédas, M. Löfgren, and W.R. Salaneck, *Electroluminescence Conjug. Polym.* **397** (1999).
- [5] J.A. Rogers, T. Someya, and Y. Huang, *Science* **327**, 1603 (2010).
- [6] C.W. Tang, and S.A. Vanslyke, *Appl. Phys. Lett.* **51**, 913–915 (1987).
- [7] G. Hong, X. Gan, C. Leonhardt, Z. Zhang, J. Seibert, J.M. Busch, and S. Bräse, *Adv. Mater.* **33** (2021).
- [8] S. Sudheendran Swayamprabha, D.K. Dubey, R.A.K. Yadav, M.R. Nagar, A. Sharma, F.C. Tung, and J.H. Jou, *Adv. Sci.* **8** (2021).
- [9] T.-H. Han, M.-R. Choi, C.-W. Jeon, Y.-H. Kim, S.-K. Kwon, and T.-W. Lee, *Sci. Adv.* **2**, 3.10 (2016).
- [10] A. van Oostrom, and L. Augustus, *Appl. Surf. Sci.* **2**, 173–186 (1979).
- [11] A.R. Brown, N.C. Greenham, J.H. Burroughes, D.D.C. Bradley, R.H. Friend, P.L. Burn, A. Kraft, and A.B. Holmes, *Chem. Phys. Lett.* **200**, 46–54 (1992).
- [12] A. Turak, *Electron. Mater.* **2**, 198–221 (2021).
- [13] C. Amruth, B. Luszczynska, W. Reka, M.Z. Szymanski, and J. Ulanski, *Polymers (Basel)* **13**, 1–16 (2021).
- [14] T.R. Briere, and A.H. Sommer, *J. Appl. Phys.* **48**, 3547–3550 (1977).
- [15] T. Ma, R. Jacobs, J. Booske, and D. Morgan, *J. Phys. Chem. C* **125**, 17400–17410 (2021).
- [16] E.G. Jeong, J.H. Kwon, K.S. Kang, S.Y. Jeong, and K.C. Choi, *J. Inf. Disp.* **21**, 19–32 (2020). 17
- [17] H.J. Jang, J.Y. Lee, J. Kim, J. Kwak, and J.H. Park, *J. Inf. Disp.* **21**, 1–9 (2020).
- [18] T. Bak, M.K. Nowotny, L.R. Sheppard, and J. Nowotny, *J. Phys. Chem. C* **112**, 12981–12987 (2008).
- [19] B.R. Lee, S. Lee, J.H. Park, E.D. Jung, J.C. Yu, Y.S. Nam, J. Heo, J.Y. Kim, B.S. Kim, and M.H. Song, *Adv. Mater.* **27**, 3553–3559 (2015).
- [20] N. Tokmoldin, N. Griffiths, D.D.C. Bradley, and S.A. Hague, *Adv. Mater.* **21**, 3475–3478 (2009).
- [21] B. Tong, J. Du, L. Yin, D. Zhang, W. Zhang, Y. Liu, Y. Wei, C. Liu, Y. Liang, D.-M. Sun, L.-P. Ma, H.-M. Cheng, and W. Ren, *Nat. Commun.* **13**, 4987 (2022).
- [22] Y. Shao, G.C. Bazan, and A.J. Heeger, *Adv. Mater.* **19**, 365–370 (2007).
- [23] D.R. Macfarlane, M. Forsyth, P.C. Howlett, J.M. Pringle, J. Sun, G. Annat, W. Neil, and E.I. Izgorodina, *Acc. Chem. Res.* **40**, 1165–1173 (2007).
- [24] R. Martín, L. Teruel, C. Aprile, J.F. Cabeza, M. Álvaro, and H. García, *Tetrahedron* **64**, 6270–6274 (2008).
- [25] S. Lee, H. Kim, and Y. Kim, *InfoMat* **3**, 61–81 (2021).
- [26] T. Sasaki, M. Hasegawa, K. Inagaki, H. Ito, K. Suzuki, T. Oono, K. Morii, T. Shimizu, and H. Fukagawa, *Nat. Commun.* **12** (2021).
- [27] S.O. Jeon, S.E. Jang, H.S. Son, and J.Y. Lee, *Adv. Mater.* **23**, 1436–1441 (2011).
- [28] S. Gong, Y.L. Chang, K. Wu, R. White, Z.H. Lu, D. Song, and C. Yang, *Chem. Mater.* **26**, 1463–1470 (2014).
- [29] C. Adachi, T. Tsutsui, and S. Saito, *Appl. Phys. Lett.* **55**, 1489–1491 (1989).
- [30] M.H. Tsai, H.W. Lin, H.C. Su, T.H. Ke, C.C. Wu, F.C. Fang, Y.L. Liao, K.T. Wong, and C.I. Wu, *Adv. Mater.* **18**, 1216–1220 (2006).
- [31] R.A.K. Yadav, D.K. Dubey, S.Z. Chen, T.W. Liang, and J.H. Jou, *Sci. Rep.* **10** (2020).
- [32] Z. Liu, W.Y. Zheng, P. Wei, Z. Xu, D. Song, B. Qiao, and S. Zhao, *RSC Adv.* **10**, 13215–13222 (2020).
- [33] Y.T. Tao, E. Balasubramaniam, A. Danel, B. Jarosz, and P. Tomasik, *Appl. Phys. Lett.* **77**, 1575–1577 (2000).
- [34] H. Yoshida, *J. Phys. Chem. C* **119**, 24459–24464 (2015).
- [35] I.G. Hill, and A. Kahn, *J. Appl. Phys.* **86**, 4515–4519 (1999).
- [36] D. Ji, J. Jang, J.H. Park, D. Kim, Y.S. Rim, D.K. Hwang, and Y.Y. Noh, *J. Inf. Disp.* **22**, 1–11 (2021).
- [37] L. Jäger, T.D. Schmidt, and W. Brütting, *AIP Adv.* **6** (2016).
- [38] L. Chen, Q. Chen, C. Wang, and Y. Li, *J. Am. Chem. Soc.* **142**, 18281–18292 (2020).
- [39] C. Liu, K. Huang, W.T. Park, M. Li, T. Yang, X. Liu, L. Liang, T. Minari, and Y.Y. Noh, *Mater. Horiz.* **4**, 608–618 (2017).
- [40] M. Knupfer, and G. Paasch, *J. Vac. Sci. Technol. A: Vac. Surf. Films* **23**, 1072–1077 (2005).
- [41] Q. Wang, Y. Zhou, H. Zheng, J. Shi, C. Li, C.Q. Su, L. Wang, C. Luo, D. Hu, J. Pei, J. Wang, J. Peng, and Y. Cao, *Org. Electron.* **12**, 1858–1863 (2011).
- [42] Z. Hu, Z. Zhong, K. Zhang, Z. Hu, C. Song, F. Huang, J. Peng, J. Wang, and Y. Cao, *NPG Asia. Mater.* **9**, e379 (2017).
- [43] J.T. Kim, J. Lee, S. Jang, Z. Yu, J.H. Park, E.D. Jung, S. Lee, M.H. Song, D.R. Whang, S. Wu, S.H. Park, D.W. Chang, and B.R. Lee, *J. Mater. Chem. A Mater.* **8**, 13501–13508 (2020).
- [44] J. Bian, S. Chen, L. Qiu, R. Tian, Y. Man, Y. Wang, S. Chen, J. Zhang, C. Duan, C. Han, and H. Xu, *Adv. Mater.* **34**, 2110547 (2022).
- [45] C. Han, R. Du, H. Xu, S. Han, P. Ma, J. Bian, C. Duan, Y. Wei, M. Sun, X. Liu, and W. Huang, *Nat. Commun.* **12**, 3640 (2021).
- [46] Y. Murat, H. Lüder, M. Köpke, J. Buhl, and M. Gerken, *J. Electron. Mater.* **50**, 2556–2564 (2021).
- [47] S. Burns, J. Macleod, T. Trang Do, P. Sonar, and S.D. Yambem, *Sci. Rep.* **7** (2017).
- [48] M.S. Kwon, J. Gierschner, S.J. Yoon, and S.Y. Park, *Adv. Mater.* **24**, 5487–5492 (2012).
- [49] H. Ishii, S. Obata, N. Niitsu, S. Watanabe, H. Goto, K. Hirose, N. Kobayashi, T. Okamoto, and J. Takeya, *Sci. Rep.* **10** (2010).
- [50] A. Hofmann, M. Schmid, and W. Brütting, *Adv. Opt. Mater.* **9** (2021).
- [51] K.M. Pelzer, L. Cheng, and L.A. Curtiss, *J. Phys. Chem. C* **121**, 237–245 (2017).
- [52] Gaussian 16;: Revision A.03, M.J. Frisch, G.W. Trucks, H.B. Schlegel, G.E. Scuseria, M.A. Robb, J.R. Cheeseman, G. Scalmani, V. Barone, G.A. Petersson, H. Nakatsuji, X. Li, M. Caricato, A.V. Marenich, J. Bloino, B.G. Janesko, R. Gomperts, B. Mennucci, H.P. Hratchian, J.V. Ortiz, A.F. Izmaylov, J.L. Sonnenberg, D. Williams-Young, F. Ding, F. Lipparini, F. Egidi, J. Goings, B. Peng, A. Petrone, T. Henderson, D. Ranasinghe, V.G. Zakrzewski, J. Gao, N. Rega,

G. Zheng, W. Liang, M. Hada, M. Ehara, K. Toyota, R. Fukuda, J. Hasegawa, M. Ishida, T. Nakajima, Y. Honda, O. Kitao, H. Nakai, T. Vreven, K. Throssell, J.A. Montgomery, J.E. Peralta, F. Ogliaro, M.J. Bearpark, J.J. Heyd, E.N. Brothers, K.N. Kudin, V.N. Staroverov, T.A. Keith, R. Kobayashi, J. Normand, K. Raghavachari, A.P. Rendell, J.C. Burant, S.S. Iyengar, J. Tomasi, M. Cossi, J.M. Millam, M. Klene, C. Adamo, R. Cammi, J.W. Ochterski,

R.L. Martin, K. Morokuma, O. Farkas, J.B. Foresman, and D.J. Fox, *Gaussian, Inc.*, Wallingford CT, 2016).

- [53] J.C. Blakesley, F.A. Castro, W. Kylberg, G.F.A. Dibb, C. Arantes, R. Valaski, M. Cremona, J.S. Kim, and J.S. Kim, *Org. Electron.* **15**, 1263–1272 (2014).
- [54] J. Sohn, D. Ko, H. Lee, J. Han, S.D. Lee, and C. Lee, *Org. Electron.* **70**, 286–291 (2019).